ELSEVIER

Catalysis Today 50 (1999) 247–259

CATALYSIS TODAY

Studies of the cerium-metal–oxygen–hydrogen system (metal=Cu, Ni)

C. Lamonier, A. Ponchel, A. D'Huysser, L. Jalowiecki-Duhamel*

Laboratoire de Catalyse Hétérogène et Homogène, URA CNRS D04020, Bât. C3, Université des Sciences et Technologies de Lille, 59655, Villeneuve d'Ascq Cedex, France

Abstract

In situ X-ray diffraction (XRD), in situ X-ray photoelectron spectroscopy (XPS), electron microscopy and thermogravimetric techniques were used to characterize CeM_xO_y mixed oxides in the oxidized and H_2 reduced state. The processes occurring during the hydrogen treatment, and the amounts of hydrogen occluded in the solids when treated at different temperatures under flowing hydrogen have also been determined. The CeM_xO_y oxides can be described as a mixture of copper oxide or nickel oxide and of ceria modified by the insertion of a part of copper or nickel in its lattice. The size of the copper oxide or nickel oxide varies considerably from clusters to a crystallized material, depending on the x value and on the experimental conditions. In the partially reduced state anionic vacancies able to receive hydrogen, probably in a hydridic form, are created in the bulk and at the surface of the solid and a reduction mechanism partly based on heterolytic dissociation of H_2 is proposed ($O^{2-}+\square+H_2 \rightarrow H^- + OH^-$). Moreover, it appears that different kinds of active sites which differ from each other in terms of the environment of nickel or copper can exist.

Keywords: X-ray diffraction; Anionic vacancies; CeM_xO_y mixed oxides

1. Introduction

The ceria-based catalysts are interesting for hydrogenation reactions [1,2], water gas shift reactions [3], CO [4] and hydrocarbon oxidation [5,6]. It appears that the common parameter for these applications is the participation of surface oxygen species/anionic vacancies [7]. As a matter of fact, on ceria-based oxides, it has already been shown that the elimination of lattice oxygen under H_2 leads to the creation of anionic vacancies [8,9] correlated to the high mobility of lattice oxygen in ceria. Further, it is well known that CeO_2 is able to store oxygen and to release it under reducing atmosphere leading to a CeO_{2-x} compound [10]. The ceria reduction and reoxidation rate is increased on metals of group VIII supported on ceria catalysts [11]. Moreover, it has been proposed that anionic vacancies associated to CeO_2 and in interaction with metallic particles are the active sites in NO and CO conversion [12] and for CO_2 transformation into methane [13,14].

Besides, the interaction of hydrogen with cerium-based oxides has also been largely studied. It has been shown that ceria is able to store hydrogen and that the hydrogen storage depends on the reduction temperature under H_2 [1,2,5–11,14–21]. Moreover, Otsuka

*Corresponding author. Tel.: +33-03-20-33-77-35; fax: +33-03-20-43-65-61; e-mail: louise.duhamel.@univ-lille1.fr

0920-5861/99/$ – see front matter
PII: S0920-5861(98)00507-0

et al. [11] have analysed the reduction and reoxidation rates on cerium oxide and a proportionality has been obtained between the quantity of H_2 produced during the oxidation step and the concentration of anionic vacancies created during the reduction step. Fierro et al. [8] estimated that during the reduction process under H_2, the incorporation of hydrogen in ceria and the elimination of lattice oxygen can affect in opposite way the mass of ceria.

In our laboratory, a $CeNi_5$ oxide, prepared by coprecipitation, was the most efficient in hydrogenation of polyunsaturated hydrocarbons and could store as much hydrogen as the $CeNi_5$ intermetallic compound [1]. Intermetallic compounds, based on rare earth elements (RE) and a transition metal such as $RENi_5$, present interesting catalytic properties and are known for their ability to absorb hydrogen and form hydrides. In all cases, when activated under air or under CO–H_2 mixture, the intermetallic compounds are transformed into supported metal catalysts [22,23]. The coprecipitation method, chosen to emphasize the possible interactions between the transition element and cerium, has been shown to be efficient, since solid solutions are present in the samples after calcination [24,25]. A series of $CeNi_xO_y$ oxides ($0 \leq x \leq 7$) have indicated the existence of three kinds of active site, depending on whether the nickel species involved in the active site is associated with hydrogen in the solid solution based on ceria, located at the surface of the metallic phase or situated at the interface of the two phases [1].

This work concerns the characterization of cerium–nickel and cerium–copper oxides in the oxidized and partially reduced state (after treatment under hydrogen) using in situ techniques (thermal analysis, XRD, XPS). The relation between the ability of the partially reduced solids for storing hydrogen, the nature of the occluded hydrogen species, and the degree of reduction of the cations will be discussed. Finally, a reduction mechanism and a model of active sites will be proposed.

2. Experimental

The mixed oxides denoted CeM_xO_y, in which M represents Cu or Ni, and x the M/Ce ratio, were prepared by coprecipitation of hydroxides from mixtures of cerium and copper or nickel nitrates using (i) NaOH:(N)CeM_xO_y [14,25], (ii) KOH:(K)CeM_xO_y [14] or (iii) triethylamine (TEA):(T)CeM_xO_y [1,24] as precipitating agent. The solids have been dried at 363 K and calcined in air at different temperatures between 573 and 1073 K (T_C). The loading has been measured by microanalysis. Pure cerium, nickel and copper oxides were also prepared and used as reference compounds.

Thermogravimetric measurements were performed using a Sartorius 4102 microbalance equipped with a flow-gas system. The calcined oxides were treated as a function of temperature under a hydrogen flow ($5\,l\,h^{-1}$) and the temperature was increased at a rate of $1.7\,K\,min^{-1}$ from room temperature to the final temperature of about 973 K. The surface areas were determined by the BET method.

The structure of the oxides was analysed in a Siemens D5000 diffractometer equipped with an Anton Paar HTK 10 chamber, and connected to a gas introduction and purification line. A position sensitive detector was used; the flow conditions and the rate of temperature increase were similar to those adopted in thermogravimetry. Apart from K_{α_2} contribution eliminated by computer post-processing, the patterns obtained were not subjected to further treatments. Owing to the use of a platinum holder, they show platinum diffraction peaks, the evolution of which with the treatment temperature T_T was taken into account in determining the exact position of the peaks of the solids analysed [14,25].

The XPS analyses were performed with a Leybold-Hereaus LHS 10 spectrometer using Al K_α radiation ($h\nu$=1486.6 eV). The details of the spectrometer and the experimental procedure are given in [14,24,25]. When necessary reduction treatments were carried out in situ up to 573 K in a preparation chamber attached via ultra high vacuum chamber, to the analysis chamber of the spectrometer. Five surface atomic ratios were obtained on the basis of the peak area intensities after correction for instrumental parameters, photoionization cross-sections and electron mean free paths.

The TEM (transmission electron microscopy) observations were performed on a microscope Philips CM 30 at 300 kV. For the observations, the ultrasonic agitated powder in alcohol suspension was deposited on a copper grid covered with a thin carbon film.

Measurement of the amount of hydrogen stored in the solid is based on the ability of this class of compounds to hydrogenate 2-methylbuta-1,3-diene (isoprene) in the absence of gaseous hydrogen, according to a dynamic method described previously [26] and applied in our laboratory to a large variety of compounds [27,28]. The pretreatment and catalytic experiments were carried out in situ at atmospheric pressure in an all-glass grease free flow apparatus. The previously calcined solid was treated first in situ under a purified hydrogen flow at various temperatures T_T between 293 and 1073 K (10 h). After each reduction step by H_2 at T_T higher than 423 K, the solid was cooled to 423 K. Isoprene was introduced at constant pressure (6 to 8 Torr−1 Torr=133.3 N m^{-2}) in an isothermal reactor (423 K) and then the mixture H_2+isoprene is replaced by a mixture of He+isoprene. The total elimination of gaseous hydrogen was followed by the use of a catharometer, after 4 min the concentration of molecular hydrogen in the gas phase was lower than 0.1%. After elimination of molecular hydrogen at 423 K, hydrogenation reaction was followed as a function of time under isoprene+helium mixture. The hydrogenation reaction involves the participation of reactive hydrogen of the solid, which can diffuse from the bulk to hydrogenate isoprene at the surface.

3. Results

3.1. Oxidized state

3.1.1. Composition and surface area

The thermal decomposition of the dried hydroxides [25] have shown that the weight loss obtained under dried air reached at 1070 K is still less than the value calculated assuming that the samples are a mixture of CeO_2 and CuO or NiO in the final state. So the transformation is not complete. Table 1 summarizes for different solids studied, the values obtained in terms of temperature of calcination and specific areas. For a given temperature, compared with the reference oxides, NiO, CuO and CeO_2, a very small amount of M increases the surface area [25]. For a given Cu/Ce or Ni/Ce ratio, the surface area decreases with the calcination temperature. This decrease is usually attributed to better crystallization of the solid.

Table 1
Temperature of calcination and specific area of some studied catalysts

Catalyst CeM_xO_y, x=M/Ce	T_C (K)	Specific area ($m^2\ g^{-1}$)
(T)CeO_2	773	79
(T)NiO	773	25
(N)CuO	673	8
(T)$CeNi_{0.2}O_y$	773	102
(T)$CeNi_{0.5}O_y$	773	83
(K)$CeNi_{0.5}O_y$	573	140
(T)$CeNi_{0.7}O_y$	773	96
(T)$CeNi_1O_y$	773	105
(K)$CeNi_5O_y$	573	190
(T)$CeCu_{0.5}O_y$	773	56
(N)$CeCu_{0.1}O_y$	673	114
(N)$CeCu_1O_y$	673	105

3.1.2. XRD

While a ceria-like phase is evidenced in all the solids analysed, crystallized CuO or NiO appears for a given value of x which can slightly be changed with the calcination temperature and/or with the coprecipitation procedure [14], in particular, for $x \geq 0.5$ in the (N)$CeCu_xO_y$ and (T)$CeNi_xO_y$ systems. A careful examination of the patterns shows that the addition of copper/nickel affects not only the broadness of the ceria peaks, particularly evident from x=0.5 [14], but also their position. With solids calcined at 773 K, Fig. 1 reports the difference between the diffraction peak positions of the reference oxide CeO_2 (JCPDS 34-394) and of the CeO_2 like phase in the mixed oxides. The lowest shift value corresponds to the ratio Ni/Ce=0.5; for higher nickel content, shifts values increase up to the value observed in CeO_2, in agreement with a segregation of the NiO and CeO_2 phases. For all the preparations studied, the evolution of the shifts of the ceria-like phase indicates that: (i) the substitution of Ce^{4+} by Ni^{2+} (which ionic radius is smaller) increases up to Ni/Ce=0.5, and for higher values of x, the NiO phase crystallizes, whereas (ii) the incorporation of Cu^{2+} in the ceria matrix increases up to Cu/Ce=2 in spite of the CuO formation, still present in $CeCu_{0.5}O_y$ [25]. Thus, the XRD analysis suggests that a solid solution is formed beginning from the coprecipitation step [14], owing to the progressive incorporation of copper/nickel in a poorly crystallized ceria lattice. If the temperature of calcination is fixed at 1073 K, the oxides are better crystallized, but shifts

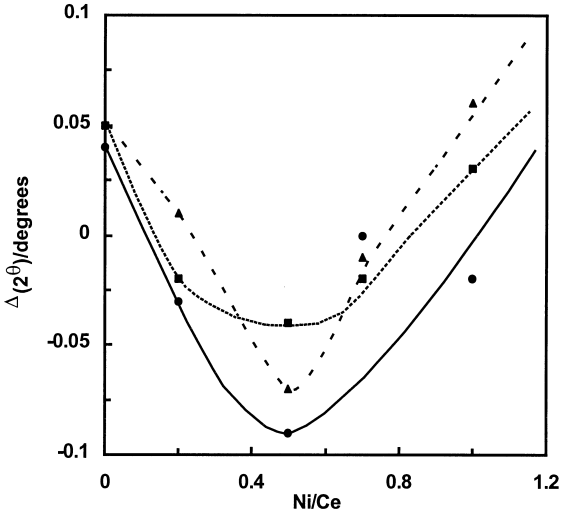

Fig. 1. Shift of the CeO_2 diffraction peaks in (T)$CeNi_xO_y$: (■) 1 1 1, (▲) 2 0 0, (●) 2 2 0. $\Delta(2\theta)$=peak position of the reference oxide CeO_2 – peak position of the CeO_2 like phase in the mixed oxide.

between the CeO_2 lines in $CeCu_xO_y$ and in the pure oxide (JCPDS 34-0394) are still observed [25], indicating that copper remains partly inserted in the CeO_2 lattice even at high temperature.

3.1.3. Electron microscopy

At low magnification, electronic microscopy shows that whatever the preparation procedure, the nickel mixed oxides, treated at 773 K under air, are constituted of large particles (up to 100 μm) and aggregates of small grains. As an example, in Fig. 2 are presented the results obtained on the (T)$CeNi_1O_y$ compound. Observations in TEM at high magnification reveal that one cannot distinguish between the surface of a large particle and the surface of an aggregate. The reference oxide CeO_2 is constituted of roundish particles homogeneous in shape and size, about 6 nm [24]. Mixed oxides with Ni/Ce>0.5 are formed with two types of particles: roundish particles with homogeneous size (about 4 nm) and particles with hexagonal shape, homogeneous in size in $CeNi_1O_y$ (8–9 nm) and various size in $CeNi_5O_y$ (15–200 nm). When the ratio Ni/Ce≤0.5, the oxides have almost the same appearance. They are constituted of roundish particles homogeneous in size (5 nm for Ni/Ce=0.5 and 4 nm for Ni/Ce=0.2). Only few crystallites of NiO are recognizable with their particular shape in $CeNi_{0.5}O_y$. To complete the information, electronic microdiffraction was used to determine the chemical structure of the small grains. The selected area was varying between 0.2 and 1 μm^2. All the diffraction spots corresponding to aggregates are generally distributed on circles. Whatever the sample, the circles related to the microdiffraction of CeO_2 are continuous in agreement with the homogeneity of the CeO_2 grains observed in TEM images. The punctuated diagrams are related to NiO for the samples with Ni/Ce≥1, suggesting that the corresponding particles are oriented and/or inhomogeneous in size. Thus, in $CeNi_1O_y$, with the hexagonal shape particles of 8–9 nm, the presence of very small particles of NiO, mixed with CeO_2 grains and so unrecognizable in TEM images, can be envisaged. In $CeNi_{0.5}O_y$, continuous diffraction circles indicate that the particle size is homogeneous despite some visible crystallites of 10 nm. In $CeNi_{0.2}O_y$, the circles corresponding to the microdiffraction of NiO are not

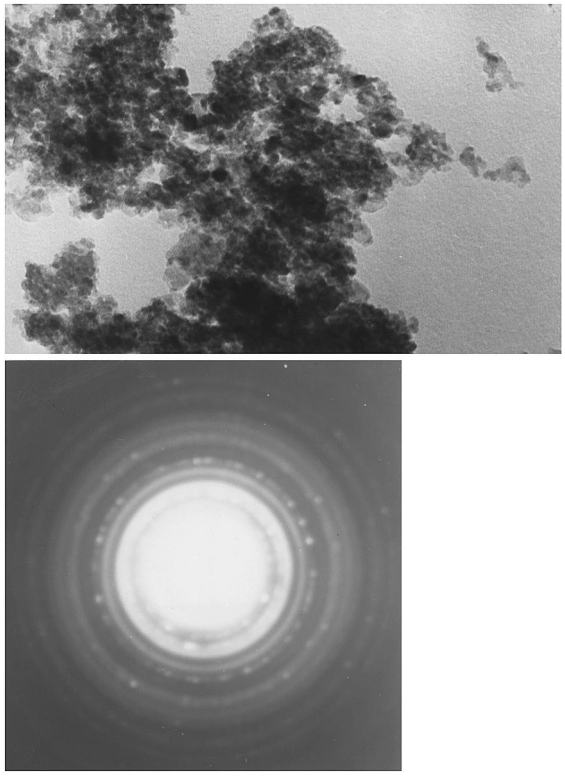

Fig. 2. Electron microscopy of the (T)$CeNi_1O_y$ compound: (a) image, (b) microdiffraction diagram obtained by TEM.

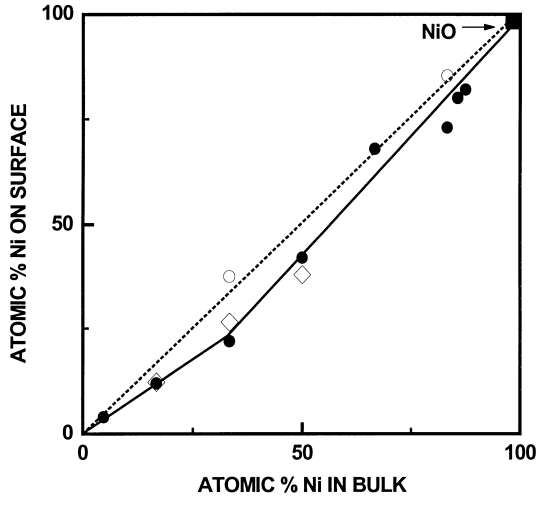

Fig. 3. Variation of the nickel surface concentration as a bulk nickel content in the fresh $CeNi_xO_y$ catalysts prepared by various coprecipitation routes. (T)$CeNi_xO_y$ series calcined at 723 K [24] (●) and 773 K (◇), (K)$CeNi_xO_y$ series calcined at 573 K (○), (T)NiO calcined at 773 K and (K)NiO calcined at 573 K (■).

complete and only few spots are visible in agreement with the low quantity of nickel in this sample.

3.1.4. XPS and Auger analysis

The XPS measurements were based on the 3d and 4d peaks for cerium, on the $2p_{3/2}$, 3p and Auger $L_3M_{4,5}M_{4,5}$ lines for copper, on the $2p_{3/2}$ lines for nickel and on the O 1s line [14,24]. Fig. 3 summarizes the XPS results on the fresh $CeNi_xO_y$ catalysts prepared by various coprecipitation routes. It can be seen that, except for the precursor calcined at 573 K, all the oxides have slightly less nickel on the surface than the bulk. The observed discontinuity near x=0.5 evidences different structural properties on both sides of this nickel concentration. Wrobel et al. [25] have classified the coprecipitated $CeNi_xO_y$ oxide precursors in two families, depending on the nickel content: the first family with $x \leq 0.5$ corresponds to a solid solution with the substitution of Ni^{2+} ions in the CeO_2 lattice and the second family with x>0.5 concerns compounds in which crystallized NiO and solid solution coexist. For $CeCu_xO_y$ mixed oxides, the Cu/Ce surface atomic ratio is a function of the depth of analysis and chemical shifts are observed on some XPS (Cu $2p_{3/2}$) and Auger (Cu $L_3M_{4,5}M_{4,5}$) lines. These results are explained by the formation of CuO clusters and/or small particles of CuO and by the incorporation of Cu^{2+} ions in the ceria matrix. When the copper content is too low (x<0.5), crystallized CuO does not form while for highest Cu/Ce values the $CeCu_xO_y$ system can be described as a mixture of a solid solution of copper in ceria in contact with copper oxide.

Finally, the CeM_xO_y mixed oxides (with M=Ni or Cu) can be described by a mixture of nickel or copper oxide and of ceria modified by the incorporation of a part of nickel or copper in its lattice. The size of the nickel oxide or copper oxide varies considerably from clusters to a crystallized material depending on the x value and on the experimental conditions (preparation conditions, calcination temperature, etc.).

3.2. Partially reduced state

3.2.1. Thermal analysis

In a previous study, we reported that after treatment under H_2 at 473 or 573 K, CeM_xO_y mixed oxides contain anionic vacancies produced by the elimination of H_2O (OH groups). All the thermograms under H_2 have been performed, and the results obtained on some compounds are presented as an example in Fig. 4. In agreement with the literature [14], up to about 373 K, the weight loss observed corresponds to the elimination of physisorbed water, while for higher treatment temperatures (T_T) anionic vacancies are created. Moreover, for temperatures higher than 423 K the observed phenomena are not the exact superimposition of those obtained for the pure reference cerium (CeO_2), nickel (NiO) and copper (CuO) oxides [14]. The thermograms of all the samples show two domains of relatively significant loss of weight, the onset of this phenomenon is marked out by the temperatures T_1 and T_2; at first, more distinct domain at about the temperature of reduction of NiO or CuO, and the other one in the 823–873 K temperature range (Table 2). The difference observed between MO (M=Cu or Ni) reduction temperature and T_1 in CeM_xO_y probably results from the presence in the oxide state of clusters or small MO aggregates which are more easily reduced. Moreover, in Table 2 has also been reported the reduction rate related to the loss of weight starting at T_1, deduced from the slope of the curve and corresponding to the reduction of the

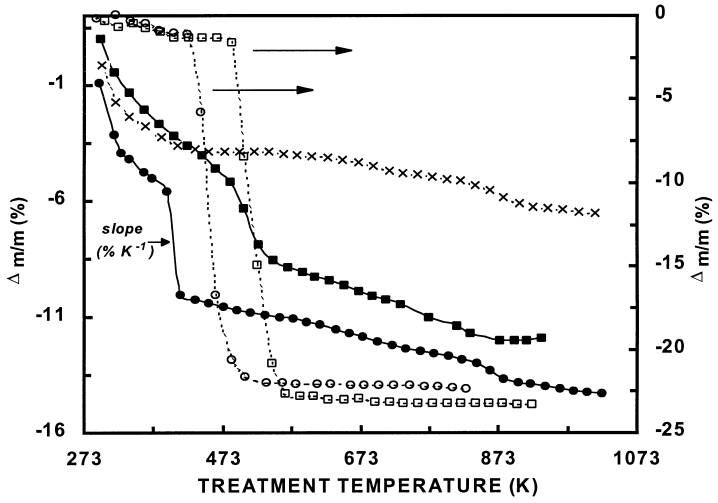

Fig. 4. Thermogravimetric profiles of CeM_xO_y compounds treated under pure hydrogen: (T)NiO (□), (N)CuO (○), (T)CeO_2 (×), (T) $CeNi_{0.5}O_y$ (■), (T)$CeCu_{0.5}O_y$ (●) previously calcined as presented in Table 1.

Table 2
Temperatures relative to the different weight losses in the mixed oxides and reference compounds

Catalyst CeM_xO_y	T_1 (K)	Reduction rate[a] (% K^{-1})	T_2 (K)
(T)CeO_2	–	–	879
(T)NiO	483	0.33	–
(N)CuO	433	≈0.4	–
(T)$CeNi_{0.2}O_y$	448	0.02	854
(T)$CeNi_{0.5}O_y$	473	0.08	815
(T)$CeNi_{0.7}O_y$	454	0.13	817
(T)$CeCu_{0.5}O_y$	393	≈1	825
(N)$CeCu_1O_y$	373	≈0.8	837

[a]Reduction rate related to the weight loss starting at T_1 and deduced from the slope of the curve.

M^{2+} cations. It appears that the M^{2+} reduction is modified, depending on the content of M^{2+} in the ceria lattice: redox processes between Ce^{4+}, Ce^{3+}, M and M^+ or M^{2+} have already been demonstrated [14].

3.2.2. *In situ XRD*

The in situ XRD has been performed on the CeM_xO_y compounds. The evolution of the XRD spectra when treated the solid under H_2 as a function of the temperature has been studied and already presented [14]. As an example in Fig. 5 are reported the results obtained on $CeNi_{0.5}O_y$. No drastic crystallographic modification is apparent. But, a careful examination shows that each diffraction line is shifted towards lower angles for treatment temperatures higher than 423 K for the $CeNi_xO_y$ compounds and for treatment temperatures higher than 373 K for $CeCu_xO_y$ compounds. In order to specify the conditions in which the expanded phase has been formed during the reduction treatment, the peak position has been plotted as a function of T_T for the most intense lines. Reported in Figs. 6 and 7 is the difference $\Delta(2\theta)$ between the initial peak position (300 K) and its position at T_T, corrected from the thermal expansion factor (the $\Delta(2\theta)$ value is given with an accuracy of $\pm 0.02^\circ$). Each curve has the same profile and three zones can be distinguished. To compare the thermal behaviour to the structural evolution of the solid, the temperatures T_1 and T_2 presented in Table 2 have been shown again in Figs. 6 and 7. The temperature T_M, deduced from XRD, at which the metallic phases appear, has also been precised in the same figures. Compared to the curves obtained on CeO_2 [14], the main change occurs in the first domain of the expansion of the ceria lattice which is maintained (zone II).

Considering in more detail the zone II, all the studies have clearly shown that several parameters influence the phenomena which occur in the bulk of the ceria-like phase: (i) The nature of the transition metal M. While the Ni–Ce association leads to only one maximum of $\Delta(2\theta)$, zone II shows two maxima for the $CeCu_xO_y$ compounds. This factor also affects

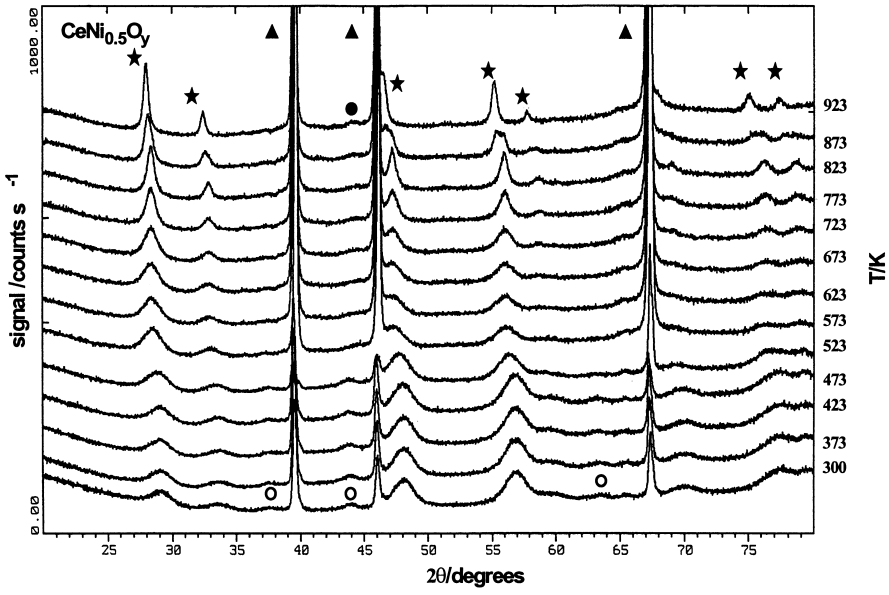

Fig. 5. XRD patterns during in situ reduction under pure hydrogen of (T)$CeNi_{0.5}O_y$ calcined at 773 K: (★) CeO_2, (○) NiO, (▲) platinum, (●) nickel.

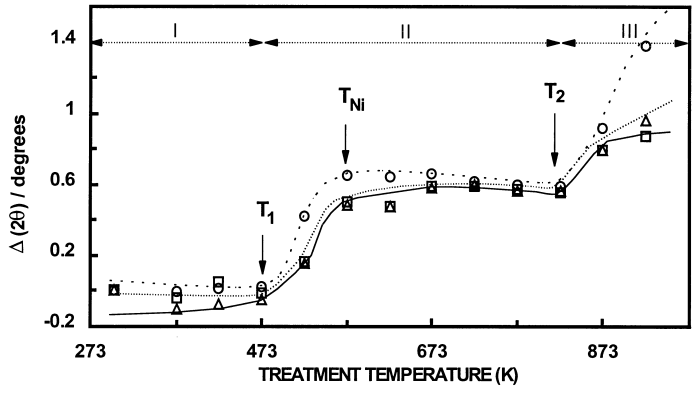

Fig. 6. Shift of the CeO_2 diffraction peaks in (T)$CeNi_{0.5}O_y$ during in situ reduction treatment under hydrogen: (□) 1 1 1, (△) 200, (○) 3 1 1. $\Delta(2\theta)$=initial peak position (300 K) – peak position at T_T.

the position of this zone in the temperature scale. (ii) The M/Ce atomic ratio; the x value also affects the temperature corresponding to the maximum of $\Delta(2\theta)$. Besides, the relative position of T_M and T_1 on the different curves leads to the following observations: (i) Whatever the M/Ce ratio, T_1 coincides with the beginning of the dilatation of ceria cell. (ii) When the solid solution is the only phase detected by XRD in the oxide precursors, the appearance of the metallic phase is associated with the end of zone II and sometimes to a decrease of the crystallographic parameter of ceria [14]. (iii) When MO is also present, T_M is shifted to T_1, and in addition to the reduction of the solid solution, free MO transforms into metal. The difference observed between T_1 and T_M implies that the metallic cation is preserved in the modified ceria phase at least for temperatures lower than T_M. At higher temperatures, a segregation of the solid solution occurs which explains the somewhat similar behaviour of CeM_xO_y and CeO_2 above 873 K.

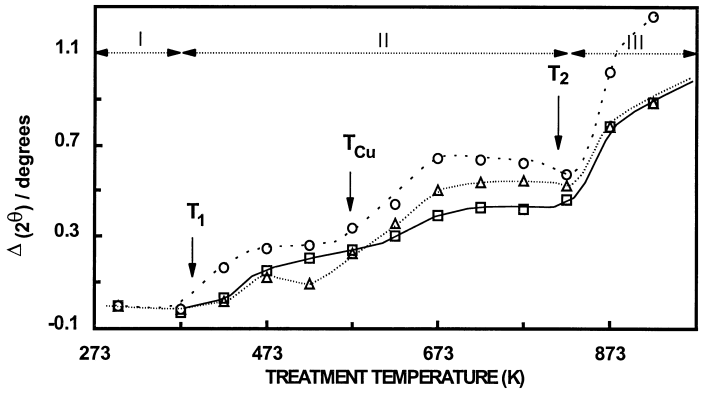

Fig. 7. Shift of the CeO_2 diffraction peaks in (T)$CeCu_{0.5}O_y$ during in situ reduction treatment under hydrogen: (□) 1 1 1, (△) 2 0 0, (○) 3 1 1.

3.2.3. XPS analysis

The XPS study reported in [14,24] has also shown that the substitution of Ce^{4+} by Ni^{2+} increases markedly the formation of Ce^{3+} species after reduction treatments performed on the $CeNi_xO_y$ series. Simultaneously there is a significant difference between the reducibility of nickel in pure nickel oxide and the mixed solids. After a treatment under H_2 at 573 K, in the former, nickel is completely converted into metallic species while in the latter NiO is completely transformed into nickel metal but only a part of nickel belonging to the solid solution is reduced. The same tendencies are observed on the reduced under H_2 at 573 K copper–cerium oxides [25]: all the Cu^{2+} is transformed into Cu^+ and Cu^0 with these two species coexisting in the solids. Moreover, progressive reduction of Ce^{4+} to Ce^{3+} coincides with the appearance of the reduced copper species and continues with the reduction of Cu^+.

3.2.4. Hydrogen H^*

After treatment under H_2 at 473 or 573 K, CeM_xO_y mixed oxides contain anionic vacancies and also some reactive hydrogen species able to hydrogenate alkadienes in absence of gaseous hydrogen [1,14]. These species are denoted H^* as we are not considering their exact charge. At 423 K under a helium+isoprene flow, alkadiene hydrogenation occurs on H_2 treated CeM_xO_y mixed oxides. It is important to note that the hydrogenation activity obtained on the untreated CeM_xO_y solid is nil. As a function of time on stream, the isoprene conversion or hydrogenation activity (HYD) is measured. The ratio $HYD_{rel.} = A_{H_t}/A_{H_0}$ (where A_{H_0} and A_{H_t} are the initial hydrogenation and the hydrogenation activity at time t) can be plotted versus time; this relative hydrogenation activity at 423 K under helium+isoprene feed decreases with time. For each solid a similar curve is obtained and by integrating this curve the extractable reactive hydrogen content of a solid can be determined if the product distribution is taken into account ($2H^*$ for monohydrogenation and $4H^*$ for dihydrogenation). In Table 3 are presented the results obtained on different solids. The hydrogen content depends on the nature and content of the cations, the preparation and pretreatment conditions (T_C).

The extractable hydrogen content of the solid is also dependent on the treatment temperature T_T under H_2. As an example, Figs. 8 and 9 show the variation in the

Table 3
H* content measured on different catalysts

Catalyst CeM_xO_y	T_C (K)	T_T (K)	[H*] (10^3 mol g^{-1})	H*/Ce[a]
(T)$CeNi_{0.2}O_y$	773	523	19.8	3.8
(T)$CeNi_{0.5}O_y$	773	523	19.5	4.1
(T)$CeNi_{0.7}O_y$	773	523	29.5	6.8
(T)$CeCu_{0.5}O_y$	773	473	11.8	2.5
(N)$CeCu_1O_y$	673	373	17.2	4.4
(N)$CeCu_1O_y$	673	473	10.9	2.8
(N)$CeCu_1O_y$	873	473	9.3	2.4
(N)$CeCu_1O_y$	1073	473	5.2	1.3

[a]The atomic weight of the catalysts has been estimated assuming that $y=2+x$: $M=M_{Ce}+xM_M+(2+x)M_O$.

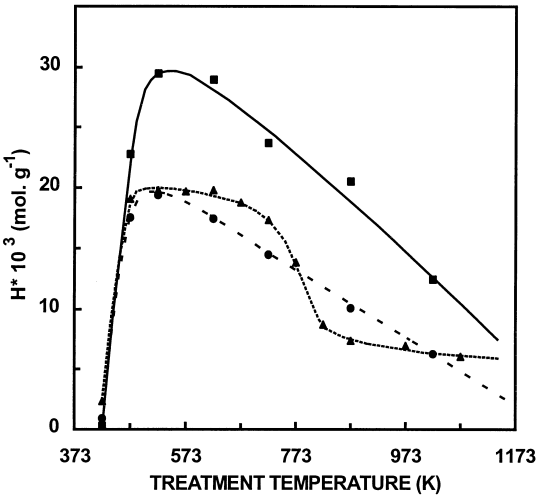

Fig. 8. Variation in the hydrogen H* species concentration as a function of the treatment temperature T_T of (T)$CeNi_xO_y$ calcined at 773 K with x=0.2 (▲), 0.5 (●), 0.7 (■).

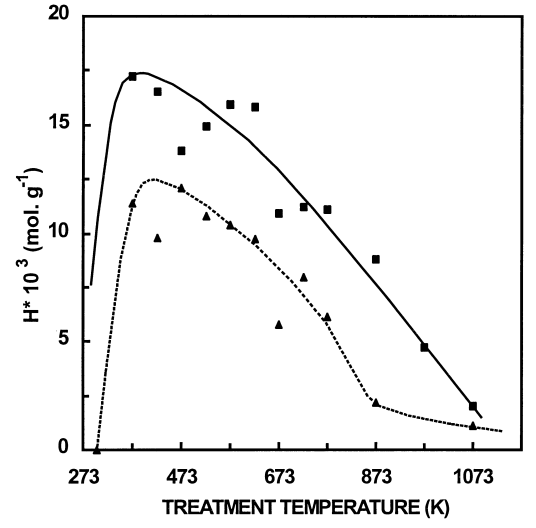

Fig. 9. Variation in the hydrogen H^* species concentration as a function of the treatment temperature T_T of (T)$CeCu_{0.5}O_y$ calcined at 773 K (▲) and of (N)$CeCu_1O_y$ calcined at 673 K (■).

hydrogen H^* species concentration as a function of the treatment temperature T_T for different (T)$CeNi_xO_y$ and (T)$CeCu_xO_y$ mixed oxides, respectively. In the series presented here, $H^*=29.5\times10^{-3}$ mol g^{-1} is obtained on (T)$CeNi_{0.7}O_y$ for T_T=523 K corresponding to the $H_{6.8}CeNi_{0.7}O_y$ compound as presented in Table 3. The values obtained are very high, as a matter of fact these mixed oxides are able to absorb higher quantities of hydrogen than the density of liquid hydrogen [2]. Moreover, for comparison, one can recall that with this dynamic method, the H^* content found with CeO_2, and CuO previously treated under H_2 at 573 and 473 K, respectively, is nil while NiO treated under H_2 at 573 K is able to store 23.9×10^{-3} mol g^{-1} of H^* species.

For the (T)$CeNi_xO_y$ catalysts (with x=0.2, 0.5 and 0.7) some reactive hydrogen species (less than 3×10^{-3} mol g^{-1}) are inserted into the solid at 423 K (Fig. 8), and at this temperature the ability of the solid to store hydrogen decreases when the value of x increases. For higher T_T the hydrogen H^* storage ability increases when x increases. The ability of the solids to store hydrogen species is maximum for a treatment temperature of about 523 K and then it decreases for temperatures higher than about 623 K. On the (T)$CeCu_xO_y$ compounds (Fig. 9), for a treatment temperature T_T=373 K the hydrogen H^* content is already very high, maximum for the (T)$CeCu_1O_y$ solid (17.2×10^{-3} mol g^{-1}).

Moreover, these H^* species present large diffusion properties, and in particular the H^* species are consumed by diffusion from the bulk to the surface of the solid [26,29]. A clear analogy exists between these results and those obtained on reduced copper based mixed oxides [28,29] which were found to be hydrogen reservoirs.

4. Discussion

On the CeM_xO_y mixed oxides, the hydrogen treatment leads to the creation of anionic vacancies and to the insertion into the solid of hydrogen species. Evidence is provided for the existence of particular reactive hydrogen species of the solid. The H^* species are able to hydrogenate alkadienes at 423 K without the presence of H_2 when the solid has been previously treated under H_2; otherwise no H^* species is found. Hence, the hydroxyl groups (OH) always present on the solid cannot justify the results obtained. Moreover, the H^* species concentration depends on the treatment temperature under H_2, almost no H^* is found for T_T lower than 353 K and the H^* content increases with the treatment temperature up to about 373–523 K depending on the solids.

For the CeM_xO_y mixed oxides, the main experimental results observed in the temperature range corresponding to the first expansion of the ceria-based lattice (zone II: 373 or 473–843 K) can be summarized as follows: (i) The insertion of Cu^{2+} or Ni^{2+} in ceria favours the expansion of the fluorite lattice under hydrogen, by shifting the corresponding zone towards lower temperatures and by increasing the expansion degree. The phenomenon is more marked for higher insertion of M^{2+} in ceria. (ii) The reduction degree of Ce^{4+} is high when the solid solution is formed [14], whereas the reduction of inserted Cu^{2+} or Ni^{2+} decreases. (iii) For Ce–Cu–O compounds, the reduction occurs in two steps and better interaction between Cu^{2+} and Ce^{3+} occurs at 473 K [14]. (iv) The amount of hydrogen extracted from the solids reduced at different T_T depends on the content of Ni^{2+} or Cu^{2+} in ceria in the oxide precursors. Finally, several hypothesis can be evoked to account for the variation of the cell parameter: the reduction of some metallic cations and/or the incorporation of hydrogen.

Taking into account previous studies which have shown that the hydrogenation mechanism can be described by a nucleophilic attack of the diene which leads to the formation of anionic intermediates [30], all the results are consistent with a heterolytic dissociation of H_2. One half of the hydrogen reservoir (H^*) consists of hydride ions H^- and the other half is protons H^+ provided by the hydroxyl groups (OH^-). Considering the relative size of H^-, and O^{2-} (1.54 and 1.32 Å, respectively), the lattice expansion observed in the reduction step under H_2 (zone II) corresponds to the substitution of an O^{2-} species by an H^- species even if the contribution of some reduced cations has also to be considered.

Therefore, the insertion in the solid of particular hydrogen species created by heterolytic splitting of H_2 can be summarized as follows:

$$H_2 + O^{2-} + \square \rightarrow H^- + OH^- \quad (1)$$

The hydroxyl groups can recombine together forming water:

$$2\,OH^- \rightarrow H_2O + O^{2-} + \square \quad (2)$$

Applied to pure ceria, the following mechanism for the reduction of CeO_2 under H_2 has already been proposed [14]:

$$2Ce^{4+} + 2O^{2-} + H_2 \rightarrow 2Ce^{3+} + 2OH^- \quad (3)$$

Apart from the reduction of the free MO oxides, when present, into the corresponding metal, the modifications registered in the reduction process when nickel or copper is added to the Ce–O system are related to the formation of anionic-defected solid solutions. Keeping in mind that the reduction of the solid solution (zone II) corresponds to the coexistence of M^0, M^+, M^{2+}, Ce^{3+}, and Ce^{4+} species and taking into account all the experimental results we propose that the reduction proceeds according to the following steps: (i) reduction of the M^{2+} ions belonging to the solid solution into M^+ or M^0 species; (ii) departure of water leading to the creation of anionic vacancies in the CeO_2 type lattice; (iii) simultaneous reoxidation of a part of the M^0 or M^+ species by reduction of the Ce^{4+} ions in their vicinity into Ce^{3+}; (iv) filling of the anionic vacancies with hydrogen, probably in the hydridic form. In addition to reaction (3), a series of reactions are proposed, which we suggest account for the reduction mechanism that takes place in the solid solution. For the cerium–nickel system:

$$Ni^{2+} + O^{2-} + H_2 \rightarrow Ni^0 + H_2O + \square \quad (4)$$

$$2Ce^{4+} + Ni^0 \leftrightarrow 2Ce^{3+} + Ni^{2+} \quad (5)$$

and for the cerium–copper system:

$$2Cu^{2+} + O^{2-} + H_2 \rightarrow 2Cu^+ + H_2O + \square \quad (6)$$

$$Ce^{4+} + Cu^+ \leftrightarrow Ce^{3+} + Cu^{2+} \quad (7)$$

$$2Cu^+ + O^{2-} + H_2 \rightarrow 2Cu^0 + H_2O + \square \quad (8)$$

$$Ce^{4+} + Cu^0 \leftrightarrow Ce^{3+} + Cu^+ \quad (9)$$

The reduction of Ni^{2+}, Cu^{2+} or Cu^+ in the solid solution is much easier than the Ce^{4+} reduction, which contributes to the creation of more anionic vacancies at lower temperatures than pure ceria and the hydrogen insertion is increased in the ceria matrix.

It has already been reported that metallic nickel is able to adsorb hydrogen [31]; therefore, for the cerium–nickel system, in addition to the route described above, the homolytic dissociation of H_2 on Ni^0 is also considered:

$$H_2 \rightarrow 2H \quad (10)$$

which favours the Ce^{4+} reduction according to

$$2Ce^{4+} + O^{2-} + 2H \rightarrow 2Ce^{3+} + H_2O + \square \qquad (11)$$

As the temperature increases the limit of stability of the complex ceria-based phase is reached, and segregation of the solid solution occurs, evidenced by the appearance of metallic nickel or copper and by a decrease in the cell parameter, particularly in the $CeCu_xO_y$ system [14]. For $CeNi_xO_y$ compounds, the transition from zone II to zone III is less evident, which is explained by the further reduction of Ce^{4+} being made easier by the homolytic dissociation of H_2.

Above 873 K, the behaviour of the solids is controlled by the reduction of ceria, the fluorite lattice of which is maintained and submitted to a novel variation of the cell parameter while the reactive and extractable hydrogen content decreases. Therefore, for treatment temperatures higher than 823 K, the increase of the lattice expansion is principally due to the reduction of the Ce^{4+} cations.

The reduction of the M^{2+} ions belonging to the solid solution into M^+ or M^0 species (4) or (6) and (8) and simultaneous reoxidation of a part of the M^0 or M^+ species by reduction of the Ce^{4+} ions in their vicinity into Ce^{3+} (5) or (7) and (9) requires the existence of particular sites where Ce and M are in close interaction. There exist two possibilities to find M in interaction with Ce : (i) in the solid solution, where M has potentially the same coordination number that Ce (site A) and (ii) at the MO particle–support interface, in such a case M can be surrounded by six oxygen atoms (site B). Some sites belonging to the solid solution, called sites A, would be constituted of superficial metal in interaction with cerium and associated with hydrogen (Scheme 1) [24]. Then the metal in strong interaction with the solid solution leads to a second

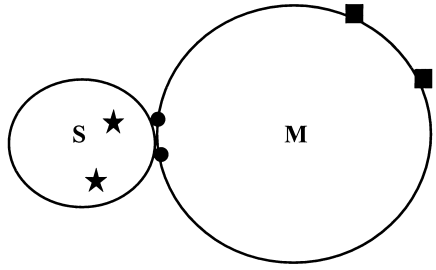

Scheme 1. Model for nickel–cerium and copper–cerium catalysts: (S) solid solution, (★) sites A, (●) sites B, (■) sites C.

type of active sites (sites B) which are different from the other superficial metal atoms belonging to the metal particles (sites C). Depending on the nature of the cations, the preparation, pretreatment and treatment conditions, different proportions of these sites (A, B, and C) are obtained. Considering only an ensemble of two cations, the sites A and B, containing hydrogen as hydride in an anionic vacancy, can be very similar as presented in Scheme 2 for which the number of anionic vacancies presented is arbitrary. The different behaviour of the catalysts [24] depends, of course, on the number of active sites but also on the different nature of the metallic cations which can have various oxidation degrees and so possess different unsaturation degrees. In particular, it has been shown that three coordinatively unsaturated sites (CUS) (^{3}M) is the prerequisite condition to obtain alkadiene hydrogenation activity, whereas two and/or four CUS sites (^{2}M,^{4} M) are related to alkadiene isomerization activity. Thus, different ensembles ^{X}M–^{Y} M′ (where X and Y are the number of unsaturations on each cation) have been proposed to be the active sites, each elementary ensemble being associated with a particular reaction [28,29]. Among all the oxides based on nickel and rare

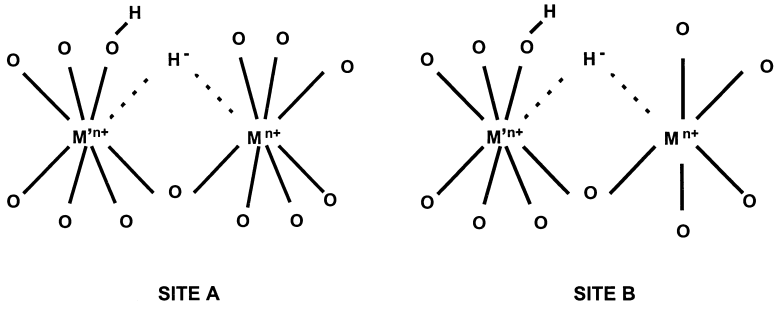

Scheme 2. Modelling of the sites A and B. The number of anionic vacancies is arbitrary: M^{n+}=Ni^{2+}, Cu^{2+}, Cu^+, $Ni^{\delta+}$; M'^{n+}=Ce^{4+}, Ce^{3+}.

earth (RE=La, Ce) prepared by coprecipitation, the Ce–Ni–O–H system has the highest hydrogen reservoir and leads to the most active hydrogenation catalysts [1,2,24]. In contrast to the other rare earth elements, the possible simultaneous presence of cerium in the two oxidation states, Ce^{3+} and Ce^{4+}, is undoubtedly a factor which is essential to the genesis of the active sites through the creation of anionic vacancies.

It is now interesting to compare the above model (Schemes 1 and 2) with the results and ideas related to nickel or other group VIII metal catalysts supported on ceria. Bearing in mind the description of the solid solution in the reduced state, one may note that the particular property of the model we propose is to gather in one picture three characteristics of the system which are sometimes displayed separately: (i) the simultaneous presence of Ce^{3+} and Ce^{4+} species already pointed out for Ni/CeO_2 [32]; (ii) the existence of anionic vacancies; (iii) the abilities of this class of solids to absorb more hydrogen than necessary for the reduction of the transition metal [33,34]. As the B sites are the most active sites for hydrogenation of benzene it supports the idea that 'the active sites are formed by a surface nickel atom at the metal–support interface in close vicinity to an anionic vacancy on the support' proposed by Herrmann et al. [13] for Ni/CeO_2 catalysts, and developed by Le Normand et al. [35] in the case of Pd/CeO_2 catalysts. This model also allows us to explain why the catalysts based on nickel and ceria contain more hydrogen than the nickel catalysts supported on more classical supports as SiO_2 or Al_2O_3 or even La_2O_3 [15] for which the reaction (5) of the reduction process does not occur. It could also be taken into account to explain the metal–support interaction found by several authors [36,37]. At last, and in a more general way, this model may be extrapolated to numerous systems already studied and based on CeO_2 and metals of group VIII, such as Pt, Pd, Rh, Ir, and to the same transition metals supported on oxides such as TiO_2 or ZrO_2 in which cations are able to have several oxidation states.

5. Conclusions

The insertion of Ni^{2+} or Cu^{2+} in ceria leads to a decrease of the reduction temperature of the host oxide and to the expansion of its lattice to a greater extent than the pure CeO_2. CeM_xO_y mixed oxides become large catalytic hydrogen reservoirs after treatment under H_2 at appropriate temperature. There is a correlation between the hydrogen content, the amount of M^{2+} inserted in the ceria matrix and the degree of reduction of the cations. An active site has been proposed based on the formation of anionic vacancies in ceria, facilitated by the incorporation of transition metal cations, the heterolytic dissociation of H_2 and redox reactions between Ce^{4+} and the transition element.

References

[1] M.P. Sohier, G. Wrobel, J.P. Bonnelle, J.P. Marcq, Appl. Catal. 84 (1992) 169.
[2] H. Diaz, J.P. Marcq, M. Pinabiau, Y. Barbaux, Eur. Patent 8 508 210 to BP France 1986.
[3] C. Padeste, N.W. Cant, D.L. Trimm, Catal. Lett. 18 (1993) 305.
[4] M.G. Sanchez, J.L. Gazquez, J. Catal. 104 (1987) 120.
[5] J.M. Herrmann, C. Hoang-Van, L. Dibansa, R.J. Harivololona, J. Catal. 159 (1996) 361.
[6] C. de Leitenburg, A. Trovarelli, J. Liorca, F. Cavani, G. Bini, Appl. Catal. 139 (1996) 161.
[7] A. Trovarelli, C. de Leitenburg, G. Dolcetti, J. Llorca, J. Catal. 151 (1995) 111.
[8] J.L.G. Fierro, J. Soria, J. Sanz, J.M. Rojo, J. Solid State Chem. 66 (1987) 154.
[9] C. Binet, A. Jadi, J.C. Lavalley, J. Chim. Phys. 89 (1992) 31.
[10] D. Bavan, J. Kordis, J. Inorg. Nucl. Chem. 26 (1964) 1509.
[11] K. Otsuka, M. Hatano, A. Morikawa, J. Catal. 79 (1983) 497.
[12] B. Harrison, A.F. Diwell, C. Halett, Platinum Metals Rev. 32 (1988) 73.
[13] J.M. Herrmann, E. Ramaroson, J.F. Tempere, M.F. Guilleux, Appl. Catal. 53 (1989) 117.
[14] G. Wrobel, C. Lamonier, A. Bennani, A. D'Huysser, A. Aboukaïs, J. Chem. Soc., Faraday Trans. 92 (1996) 2001.
[15] J. Barrault, A. Alouche, V. Paul-Boncour, L. Hilaire, A. Percheron-Guegan, Appl. Catal. 46 (1989) 269.
[16] J. Cunningham, S. O'Brien, J. Sanz, J.M. Rojo, J.A. Soria, J.L.G. Fierro, J. Mol. Catal. 57 (1990) 379.
[17] A. Laachir, V. Perrichon, A. Badri, J. Lamotte, E. Catherine, J.C. Lavalley, J. El Fallah, L. Hilaire, F. Le Normand, E. Quéméré, G.N. Sauvion, O. Touret, J. Chem. Soc., Faraday Trans. 87 (1991) 1601.
[18] V. Perrichon, A. Laachir, G. Bergeret, R. Frety, L. Tournayan, O. Touret, J. Chem. Soc., Faraday Trans. 90 (1994) 773.
[19] G. Ranga-Rao, J. Kaspar, S. Meriani, R. di Monte, M. Graziani, Catal. Lett. 24 (1994) 107.
[20] A. Bensalem, F. Bozon-Verduraz, V. Perrichon, J. Chem. Soc., Faraday Trans. 91 (1995) 2185.

[21] A. Trovarelli, F. Zamar, J. Llorca, C. de Leitenburg, G. Dolcetti, J.T. Kiss, J. Catal. 169 (1997) 490.
[22] E. Baglin, G.B. Atkinson, L.J. Nicks, US Patent 4 (1980) 630.
[23] A. Ellatar, W.E. Wallace, R.S. Craig, Adv. Chem. Ser. 178 (1979) 7.
[24] G. Wrobel, M.P. Sohier, A. D'Huysser, J.P. Bonnelle, J.P. Marcq, Appl. Catal. 101 (1993) 73.
[25] C. Lamonier, A. Bennani, A. D'Huysser, A. Aboukaïs, G. Wrobel, J. Chem. Soc., Faraday Trans. 92 (1996) 131.
[26] L. Jalowiecki, M. Daage, J.P. Bonnelle, A. Tchen, Appl. Catal. 16 (1985) 1.
[27] L. Jalowiecki, J. Grimblot, J.P. Bonnelle, J. Catal. 126 (1990) 101.
[28] A. Sene, L. Jalowiecki-Duhamel, G. Wrobel, J.P. Bonnelle, J. Catal. 144 (1993) 544.
[29] L. Jalowiecki, G. Wrobel, M. Daage, J.P. Bonnelle, J. Catal. 107 (1987) 375.
[30] M. Daage, J.P. Bonnelle, Appl. Catal. 16 (1985) 355.
[31] S. Kacimi, D. Duprez, J.A. Dalmon, J. Chim. Phys. 94 (1997) 535.
[32] I. Akalay, M.F. Guilleux, J.F. Tempere, D. Delafosse, J. Chem. Soc., Faraday Trans. 83 (1987) 1137.
[33] M.D. Mitchell, M.A. Vannice, Ind. Eng. Chem. Fundam. 23 (1984) 88.
[34] L. Tournayan, N.R. Marcilio, R. Frety, Appl. Catal. 78 (1991) 31.
[35] F. Le Normand, J. Barrault, R. Breault, L. Hilaire, A. Kienneman, J. Phys. Chem. 95 (1991) 257.
[36] A. Maubert, G.A. Martin, H. Praliaud, P. Turlier, React. Kinet. Catal. Lett. 24 (1984) 183.
[37] P. Turlier, H. Praliaud, P. Moral, G.A. Martin, J.A. Dalmon, Appl. Catal. 19 (1985) 287.